Shallow impurity states in InSb in magnetic fields: High-field donor states and acceptor states

P. J. Lin-Chung and B. W. Henvis
Naval Research Laboratory, Washington, D. C. 20375
(Received 11 November 1974)

The high-field donor and acceptor states associated with Landau ladders are determined using the effective-mass approximation. Nonparabolic effects as well as band-band interaction are included in this calculation. Based on the calculated results, the coexisting feature of the Landau series and Rydberg series is reexamined. A quantitative comparison with the magneto-optical measurements is made in order to obtain information about the central-cell correction and nonparabolic effects. Selection rules for optical transitions and Raman transitions are also derived.

I. INTRODUCTION

The occurrence of small effective masses and a high-valued dielectric function combine to make magnetic-field effects on impurity levels in InSb particularly interesting. Indeed, there have been a significant number and variety of experimental studies designed to probe the magnetic field dependence of impurity levels in InSb.[1-7] However, previous theoretical treatments[8-11] have been confined to donor impurity states only. In those works, the Coulombic aspects of the problem have been emphasized without inclusion of the details of InSb band structure that are handled in theoretical treatments of magnetic-field effects on free-carrier levels.[12,13] The purposes of this paper are to include such details of the InSb band structure in the effective-mass approximation and to extend the theory to also include acceptor levels. Thus, the theory incorporates the nonparabolic and and the warping behavior of the conduction and valence bands, as well as consideration of quantum effects due to light- and heavy-hole valence-band degeneracy. The aim is to test the isolated-hydrogenic-impurity model treated in the effective-mass approximation by comparing the results with magneto-optical data quantitatively.

The organization of this paper is as follows: In Sec. II, we present the general formalism for high-field impurity levels. The results of the evaluation, as well as their comparison with experiment, for donor and acceptor states, are given in Secs. III and IV, respectively. Because of the recent upsurge of interest in electronic Raman scattering in semiconductors, we have also investigated the impurity-shifted Raman scattering from Landau levels. A discussion for the latter is given in Sec. V.

II. GENERAL FORMALISM

In InSb, the conduction- and valence-band edges all occur at the center of the Brillonim zone; the conduction band is doubly degenerate, whereas the valence band, under spin-orbit interaction, splits into a fourfold-degenerate heavy-hole–light-hole band and a doubly degenerate spin-orbit split-off band.

Following Pidgeon and Brown,[12] who first treated the magnetic energy levels using a modified Luttinger and Kohn effective-mass method,[14] we classify the energy levels for free carriers in a magnetic field as Landau a and b ladders associated with the conduction band, light-hole band, heavy-hold band, etc., where loosely speaking, a and b correspond to "spin-up" and "spin-down" levels, respectively. Hereafter, we use the notations $a^c(N)$, $b^c(N)$, $a^l(N)$, $b^l(N)$, $a^h(N)$, $b^h(N)$ for these levels; the superscripts c, l, h refer to conduction, light-hole, and heavy-hole band, respectively. N represents the quantum number of the Landau level. Actually, the Landau levels associated with each hold band contain a strong mixture of light-hole band and heavy-hole band character. We use $a^l(N)$, $b^l(N)$ just to indicate the set of ladders which have wider energy separations, and $a^h(N)$, $b^h(N)$ to indicate those with narrower energy separation, for convenience.

Again, following Pidgeon and Brown,[12] we write a set of coupled effective-mass equations in the presence of a magnetic field in atomic units

$$\sum_{j'}\{D^{\alpha\beta}_{jj'}k_\alpha k_\beta + \Pi^{\alpha}_{jj'}k_\alpha + \tfrac{1}{2}S(\sigma_3)_{jj'} + [(\vec{\sigma}\times\vec{\nabla}V)\cdot\vec{p}]_{jj'}/4C^2 + \epsilon_{j'}\delta_{jj'}\}f_{j'}(\vec{r}) = Ef_j(\vec{r}) \,, \tag{1}$$

where j' runs over the two conduction, two heavy-hole, two light-hole, and two spin-orbit split-off band states ($j'=1-8$). Here $\epsilon_{j'}$ is the energy of the jth band-edge state; $D^{\alpha\beta}_{jj'}$, $\Pi^{\alpha}_{jj'}$ are, respectively, the inverse-effective-mass matrix element and modified-momentum matrix element between band j and j' at $k=0$;

$$D^{\alpha\beta}_{jj'} \equiv \tfrac{1}{2}\delta_{jj'}\delta_{\alpha\beta} + \sum_i [\Pi^{\alpha}_{ji}\Pi^{\beta}_{ij'}/(\epsilon'_0 - \epsilon_i)] \,, \tag{2}$$

$$\Pi_{jj'} \equiv \int U_{j0}^{*}(\vec{r})[\vec{p} - (4C^2)^{-1}(\vec{\nabla} V \times \vec{\sigma})] U_{j'0}(\vec{r})\, d\vec{r} \,. \quad (3)$$

ϵ_0' in Eq. (2) represents an average energy of the set of states j. The first term in Eq. (1) represents the effective-mass term; the second term is the $\vec{k}\cdot\vec{p}$ interaction term; the third term is the spin magnetic energy; the fourth term is the spin-orbit coupling.

The wave function of the free carriers in a magnetic field is expressed as a linear combination of the products of envelope functions $f_j(r)$ and the jth band-edge Bloch function $U_{j0}(\vec{r})$,

$$\psi(\vec{r}) = \sum_j f_j(\vec{r}) U_{j0}(\vec{r}) \,. \quad (4)$$

This type of wave function was used in order to take into account the nonparabolic and warping behavior of the conduction and valence bands from the very beginning.

Generally, the envelope functions $f_j(\vec{r})$, which appear in Eq. (1) and Eq. (4), may be expanded in terms of linear combinations of a complete set of harmonic oscillator functions Φ_n. However, if in Eq. (1), one ignores a small odd part[15] which comes from the inversion asymmetry of the zinc-blende structure and a small anisotropic part[15] which prevents the constant energy contours perpendicular to the magnetic field from being circular, Eq. (4) may be reduced to a simple form

$$\psi(\vec{r}) = \sum_j f_j(\vec{r}) U_{j,0}(\vec{r}) = \sum_j A_j \Phi_n U_{j,0} \,, \quad (5a)$$

where n has a fixed relation to j. Instead of having a double summation n and j, Eq. (5a) has now only a single summation. Thus, the dimension of the magnetic matrix Hamiltonian is reduced from infinity by infinity to 8×8. Furthermore, if one follows Luttinger and chooses the magnetic field H to be in the $(1\bar{1}0)$ plane, a small part of the anisotropy which cannot be treated exactly is excluded. Then the 8×8 matrix can be reduced further into two 4×4 matrices.

The Φ_n in Eq. (5a) are the eigenfunctions of the Hamiltonian

$$H\Phi_n = (a^{\dagger} a + \tfrac{1}{2})\hbar\omega \Phi_n \,, \quad (5b)$$

where

$$a^{\dagger} = (1/2\gamma)^{1/2}(k_x + ik_y) \,,$$

$$a = (1/2\gamma)^{1/2}(k_x - ik_y) \,,$$

$$\vec{k} = \vec{p} - e\vec{A}/c \,,$$

$$\gamma \equiv \tfrac{1}{2}\hbar\omega_c / R^{*}$$

(R^{*} is the effective rydberg).

At first sight, Φ_n look like one-dimensional harmonic oscillator functions. Actually, if we use the the symmetric gauge $\vec{A} = \frac{1}{2}H(-y, x, 0)$, we will see that Φ_n are in fact two-dimensional functions of (x, y) or (ρ, ϕ) and should have the following form:

$$\Phi_n = \Phi_{NM}(\sigma, \phi)$$
$$= c e^{iM\phi} e^{-\sigma/2} \sigma^{1/2|M|} L_{N-(M-|M|)/2}^{|M|}(\sigma) \,, \quad (5c)$$

where $\sigma = \frac{1}{2}\gamma\rho^2$, $L_Q^P(\sigma)$ are associate Laguerre polynomials, and c is a normalization constant. $C^2 = (\gamma/2\pi)[N - \frac{1}{2}(M + |M|)]!/\{[N - \frac{1}{2}(M - |M|)]!\}^3$. We can easily show that

$$a^{\dagger}\Phi_{N,M} = \pm i(N+1)^{1/2}\Phi_{N+1,M+1} \,,$$
$$a\Phi_{N,M} = \mp i N^{1/2}\Phi_{N-1,M-1} \,. \quad (5d)$$

N is now the quantum number associated with the Landau level, and M is the zth component of the angular momentum.

As a result, the envelope functions associated with the a, b ladders when written in a column vector form become

$$f_a(N, M) = \begin{pmatrix} A_1\Phi_{N,M} \\ A_3\Phi_{N-1,M-1} \\ A_5\Phi_{N+1,M+1} \\ A_7\Phi_{N+1,M+1} \end{pmatrix} \,, \quad (6a)$$

$$f_b(N, M) = \begin{pmatrix} A_2\Phi_{N,M} \\ A_6\Phi_{N-1,M-1} \\ A_4\Phi_{N+1,M+1} \\ A_8\Phi_{N-1,M-1} \end{pmatrix} \,, \quad (6b)$$

Here $M \leq N$. The energy levels belonging to $\Phi_{N,M}$ may be labeled by N and are degenerate for different M. Note that the vector bases for these two solutions are different; they are $U_{1,0}$, $U_{3,0}$, $U_{5,0}$, $U_{7,0}$ and $U_{2,0}$, $U_{6,0}$, $U_{4,0}$, $U_{8,0}$, respectively.

Equations (6) holds for $N \geq 1$. For $N = -1$, we set $A_1 = A_3 = A_2 = A_6 = A_8 = 0$, while for $N = 0$, we set $A_3 = A_6 = A_8 = 0$.

The energies and wave-function coefficients of the $a^c(N)$, $b^c(N)$, $a^l(N)$, $b^l(N)$ states in InSb in magnetic fields up to 100 kG were obtained in previous calculations.[16] In particular, we list those solutions for $H = 50$ kOe in Table I. (Since the energies are degenerate with respect to M, the values shown are independent of M.)

As for the bound charge carrier state in a magnetic field when impurity centers are present, we follow Wallis and Bowlden's treatment[8] and adopt a variational envelope function. This envelope function is related to the free-charge-carrier envelope function $f(N, M)$ given above.

$$F(N, M, \lambda) = f(N, M) P_{\lambda}(Z) e^{-1/4\gamma\epsilon^2 Z^2} \,, \quad (7)$$

where ϵ is the parameter determined variationally, and γ is the magnetic-field parameter defined by $\gamma \equiv \frac{1}{2}\hbar\omega_c / R^{*}$. $P_{\lambda}(Z)$ represents a set of orthogonal polynomials of Z of order λ. For example, the

TABLE I. Energies and wave-function parameters of the free-carrier Landau levels at $B = 50$ kG, which are used in the present calculation.

	Conduction band									
N	E_a (meV)	E_b (meV)	A_1	A_3	A_5	A_7	A_2	A_6	A_4	A_8
0	249	260	0.983	0	0.175	0.059	0.959	0	0.285	0
1	281	289	0.939	0.261	0.209	0.077	0.925	0.144	0.347	0.053
2	308	315	0.914	0.326	0.226	0.090	0.904	0.181	0.380	0.072
	Light-hole band									
N	E_a (meV)	E_b (meV)	A_1	A_3	A_5	A_7	A_2	A_6	A_4	A_8
−1	−1.49	−1.43	0	0	1	0	0	0	1	0
0	−11.9	−26.5	−0.175	0	0.984	−0.013	−0.285	0	0.959	0
1	−38.6	−52.8	−0.331	0.679	0.655	−0.037	−0.374	0.328	0.867	−0.031
2	−62.7	−75.5	−0.392	0.719	0.571	−0.056	−0.418	0.373	0.826	−0.051

P_λ have the following form:

$$P_0(Z) = (\epsilon^2\gamma/2\pi)^{1/4}, \quad P_1(Z) = (\epsilon^6\gamma^3/2\pi)^{1/4} Z. \quad (8)$$

The last factor in Eq. (7) is an exponential function of Z similar to a hydrogenic wave function. Unlike Larsen[9] and Baldereschi *et al.*[17] who chose a trial function depending on two parameters in order to improve the solution for low magnetic fields, we use only one parameter ϵ in our trial function so that the required integrations can be performed analytically. In the range of magnetic field under consideration here, this will not introduce any serious error.

The presence of an impurity center gives rise to a Coulombic potential screened by the static dielectric constant of the crystal. Usually, in the presence of a magnetic field, the polarization of free carriers also introduces additional screening. However, this screening is negligibly small for sufficiently low carrier concentration. Under this condition, if the energy is expressed in units of the effective rydberg R^*, and length in units of the effective Bohr radius, the impurity potential in cylindrical coordinates is simply $-2(\rho^2+Z^2)^{-1/2}$.

The bound-impurity-state envelope function will then satisfy the following effective-mass equation:

$$\left(H_0 - \frac{2}{(\rho^2+Z^2)^{1/2}}\right) F(N,M,\lambda) = E(N,M,\lambda)\, F(N,M,\lambda) \,. \quad (9)$$

Here H_0 is the Hamiltonian for free carrier in an external magnetic field, i.e.,

$$H_0 f(N,M) = E(N,M) f(N,M) \,. \quad (10)$$

Equations (10) and (1) are equivalent.

The type of trial envelope function in Eq. (7) is valid for $\gamma \gg 1$. Since the effective mass for the heavy hole is very large, the field parameter γ for the heavy-hole is much smaller than one, even for magnetic fields up to a few hundred kOe. Thus, Eq. (7) is not an appropriate form for high-field impurity states associated with heavy-hole Landau ladders. The low-field solutions will be more suitable for the heavy-hole related states in the magnetic-field range under consideration.[18]

We have solved Eq. (9) and obtained the binding energies $E^B(N,M,\lambda)$ for the high-field impurity states, as well as the variational parameter ϵ as a function of magnetic field.

The binding energy is defined by

$$E^B(N,M,\lambda) = E(N,M,\lambda) - E(N,M) \,. \quad (11)$$

After performing analytical integrations, solutions of Eqs. (9) and (10) for the a and b sets of states lead to

$$E_a^B(N,M,\lambda) = K(\lambda) + A_1^2 G(N,M,\lambda) + A_3^2 G(N-1, M-1, \lambda) + (A_5^2 + A_7^2) G(N+1, M+1, \lambda) \,, \quad (12)$$

when

$$K'(\lambda) + A_1^2 G'(N,M,\lambda) + A_3^2 G'(N-1, M-1, \lambda) + (A_5^2 + A_7^2) G'(N+1, M+1, \lambda) = 0 \,; \quad (13)$$

$$E_b^B(N, M, \lambda) = K(\lambda) + A_2^2 G(N,M,\lambda) + A_4^2 G(N+1, M+1, \lambda) + (A_6^2 + A_8^2) G(N-1, M-1, \lambda) \,, \quad (14)$$

when

$$K'(\lambda) + A_2^2 G'(N, M, \lambda) + A_4^2 G'(N+1, M+1, \lambda) + (A_6^2 + A_8^2) G'(N-1, M-1, \lambda) = 0. \quad (15)$$

In the above expression,

$$K(0) = \tfrac{1}{4}\gamma\epsilon^2 \,, \quad K'(0) = \tfrac{1}{2}\gamma\epsilon \,,$$
$$K(1) = \tfrac{1}{4}3\gamma\epsilon^2 \,, \quad K'(1) = \tfrac{1}{2}3\gamma\epsilon \,.$$

The integrals $G(N,M,\lambda)$ and $G'(N,M,\lambda)$ are given in Table II.

Equations (13) and (15) give the relationship be-

TABLE II. Expressions for the $G(N,M,\lambda)$ and $G'(N,M,\lambda)$ integrals $G(N,M,\lambda)=\langle\phi_{NM}P_\lambda(z)\exp(-1/4\gamma\epsilon^2Z^2)\times|-2(\rho^2+z^2)^{-1/2}|\phi_{NM}P_\lambda(z)\exp(-1/4\gamma\epsilon^2z^2)\rangle$. In the following expressions, $\Gamma\equiv-(\gamma/2\pi)^{1/2}$, $S(\epsilon)\equiv[1/(1-\epsilon^2)^{1/2}]\times\ln[1+(1-\epsilon^2)^{1/2}]/1-(1-\epsilon^2)^{1/2}]$.

$G(N,M,\lambda)\equiv d/d\epsilon\, G(N,M,\lambda)$

$G(0,0,0)=2\epsilon S(\epsilon)\Gamma$

$G'(0,0,0)=2[S(\epsilon)-2](1-\epsilon^2)^{-1}\Gamma$

$G(1,1,0)=2\epsilon[(1-\frac{1}{2}\epsilon^2)S(\epsilon)-1](1-\epsilon^2)^{-1}\Gamma$

$G'(1,1,0)=[(2+\epsilon^2)S(\epsilon)-6](1-\epsilon^2)^{-2}\Gamma$

$G(0,0,1)=4\epsilon[-\frac{1}{2}\epsilon S(\epsilon)+1](1-\epsilon^2)^{-1}\Gamma$

$G'(0,0,1)=4[-\frac{3}{2}\epsilon^2S(\epsilon)+1+2\epsilon^2](1-\epsilon^2)^{-2}\Gamma$

$G(1,1,1)=\epsilon[(-4\epsilon^2+\epsilon^4)S(\epsilon)+4+2\epsilon^2](1-\epsilon^2)^{-2}\Gamma$

$G'(1,1,1)=[(-12\epsilon^2-3\epsilon^4)S(\epsilon)+4+26\epsilon^2](1-\epsilon^2)^{-3}\Gamma$

$G(1,0,0)=\epsilon[(2-2\epsilon^2+\frac{3}{2}\epsilon^4)S(\epsilon)-2-\epsilon^2](1-\epsilon^2)^{-2}\Gamma$

$G'(1,0,0)=[(2+2\epsilon^2+\frac{7}{2}\epsilon^4)S(\epsilon)-6-5\epsilon^2-4\epsilon^4](1-\epsilon^2)^{-3}\Gamma$

$G(2,1,0)=\epsilon[(2-3\epsilon^2+\frac{15}{4}\epsilon^4-\frac{7}{8}\epsilon^6)S(\epsilon)-3+\epsilon^2-\frac{7}{4}\epsilon^4](1-\epsilon^2)^{-3}\Gamma$

$G'(2,1,0)=[(2+3\epsilon^2+\frac{27}{4}\epsilon^4+\frac{11}{8}\epsilon^6)S(\epsilon)-7-6\epsilon^2-\frac{53}{4}\epsilon^4](1-\epsilon^2)^{-4}\Gamma$

$G(2,2,0)=\epsilon[(\frac{3}{4}\epsilon^4-2\epsilon^2+2)S(\epsilon)-3+\frac{3}{2}\epsilon^2](1-\epsilon^2)^{-2}\Gamma$

$G'(2,2,0)=[(2+2\epsilon^2-\frac{1}{4}\epsilon^4)S(\epsilon)-7-\frac{1}{2}\epsilon^2](1-\epsilon^2)^{-3}\Gamma$

$G(2,0,0)=\epsilon[(4-8\epsilon^2+15\epsilon^4-7\epsilon^6+\frac{41}{16}\epsilon^8)S(\epsilon)-6+\epsilon^2-\frac{21}{4}\epsilon^4-\frac{23}{8}\epsilon^6](1-\epsilon^2)^{-4}\Gamma$

$G'(2,0,0)=[(4+8\epsilon^2+27\epsilon^4+11\epsilon^6+\frac{145}{16}\epsilon^8)S(\epsilon)-14-23\epsilon^2-\frac{205}{4}\epsilon^4-\frac{175}{8}\epsilon^6-8\epsilon^8](1-\epsilon^2)^{-5}\Gamma$

$G(3,3,0)=\epsilon[(2-3\epsilon^2+\frac{9}{4}\epsilon^4-\frac{5}{8}\epsilon^6)S(\epsilon)-\frac{11}{3}+\frac{11}{3}\epsilon^2-\frac{5}{4}\epsilon^4](1-\epsilon^2)^{-3}\Gamma$

$G'(3,3,0)=[(2+3\epsilon^2-\frac{3}{4}\epsilon^2+\frac{1}{8}\epsilon^6)S(\epsilon)-\frac{23}{3}-\frac{4}{3}\epsilon^2+\frac{1}{4}\epsilon^4](1-\epsilon^2)^{-4}\Gamma$

$G(3,2,0)=\epsilon[(2-4\epsilon^2+\frac{27}{4}\epsilon^4-\frac{13}{4}\epsilon^6+\frac{11}{16}\epsilon^8)S(\epsilon)-\frac{11}{3}+\frac{7}{2}\epsilon^2-\frac{67}{12}\epsilon^4+\frac{11}{8}\epsilon^6](1-\epsilon^2)^{-4}\Gamma$

$G'(3,2,0)=[(2+4\epsilon^2+\frac{39}{4}\epsilon^4+\frac{17}{4}\epsilon^6-\frac{5}{16}\epsilon^8)S(\epsilon)-\frac{23}{3}-\frac{43}{6}\epsilon^2-\frac{287}{12}\epsilon^4-\frac{5}{8}\epsilon^6](1-\epsilon^2)^{-5}\Gamma$

$G(2,2,1)=2\epsilon[(-3\epsilon^2+\frac{3}{2}\epsilon^4-\frac{3}{8}\epsilon^6)S(\epsilon)+2+\frac{5}{2}\epsilon^2-\frac{3}{4}\epsilon^4](1-\epsilon^2)^{-3}\Gamma$

$G'(2,2,1)=[(-18\epsilon^2-9\epsilon^4+\frac{3}{4}\epsilon^6)S(\epsilon)+4+47\epsilon^2+\frac{3}{2}\epsilon^4](1-\epsilon^2)^{-4}\Gamma$

$G(0,-1,1)=G(1,1,1)$, $G'(0,-1,1)=G'(1,1,1)$

$G(0,-1,0)=G(1,1,0)$, $G'(0,-1,0)=G'(1,1,0)$

$G(1,-1,0)=G(2,1,0)$, $G'(1,-1,0)=G'(2,1,0)$

$G(0,-2,0)=G(2,2,0)$, $G'(0,-2,0)=G'(2,2,0)$

tween the variational parameter ϵ and the field parameter γ for the a-set and b-set impurity states.

III. HIGH-FIELD DONOR STATES

The magnetic field dependences of the binding energy and variational parameter for the donor states associated with the conduction a Landau ladder are shown in Figs. 1 and 2. The shape of the curves for $N=0$ in Fig. 1 agrees quite well with those obtained in Ref. 8. As we can see, the binding energies for $\lambda=0$ states increase to infinity as $(\ln H)^2$ when $\gamma\to\infty$, while those for $\lambda=1$ states (odd in Z) tend to finite binding energies. This is, presumably, due to the fact that the wave functions are even or odd in Z. On the other hand, the variational parameters ϵ for all the states have similar magnetic field dependences.

From Eq. (12), the (110) and $(0\bar{1}0)$ states would have the same binding energy $E^B=K(0)+A_1^2G(110)$ if the nonparabolicity were ignored (i.e., if $A_3=A_5=A_7=0$). Note that, in Fig. 1, these two states now have different binding energies. The field dependences of these binding energies look similar. Another two sets of levels with only very small differences in binding energies are the (220), $(0\bar{2}0)$, and (210), $(1\bar{1}0)$ levels. The binding energy of the $(000)a$ state at $H=25$ kOe, being 2.35 meV is increased by a factor of 4 compared with the zero-field binding energy 0.586 meV. This exactly coincides with Yafet's prediction[2] and suggests that free charge carriers can become bound to ionized donors in moderate to strong magnetic fields.

The numerical values for the binding energies are listed in Table III, and the energy-level diagram is given in Fig. 3 for a magnetic field of 50 kG. As shown in Fig. 3, the impurity levels associated with Landau a ladders and those associated with Landau b ladders have the same orderings, and the binding energies for $(NM\lambda)a$ and $(NM\lambda)b$ are nearly equal. Earlier work on the transmission and photoconductivity spectra[4] revealed three prominent impurity transitions; they are the transitions from the ground state $(000)a$ to the excited states $(0\bar{1}0)a$, $(001)a$, and $(010)a$. The results of our calculation and several other calculations are compared with the experimental excitation spectra in Fig. 4. The field dependence of the three observed prominent impurity transition energies are shown by solid circles. The theoretically calculated re-

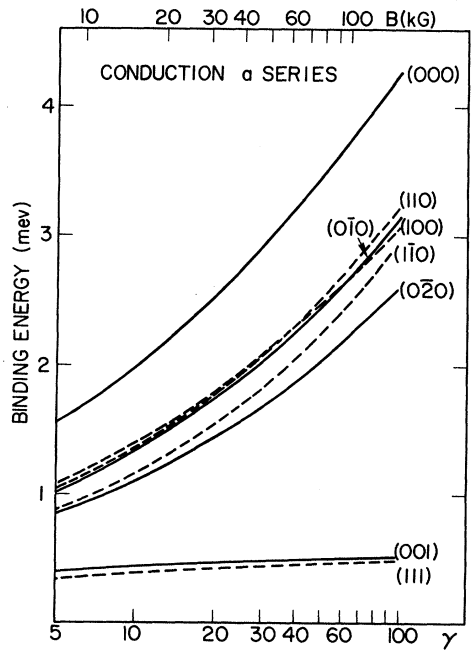

FIG. 1. Binding energy as a function of γ for the high-field impurity states $(NM\lambda)a$ associated with the conduction a Landau ladder in InSb. Full curves are for $N=0$; dashed curves are for $N=1$.

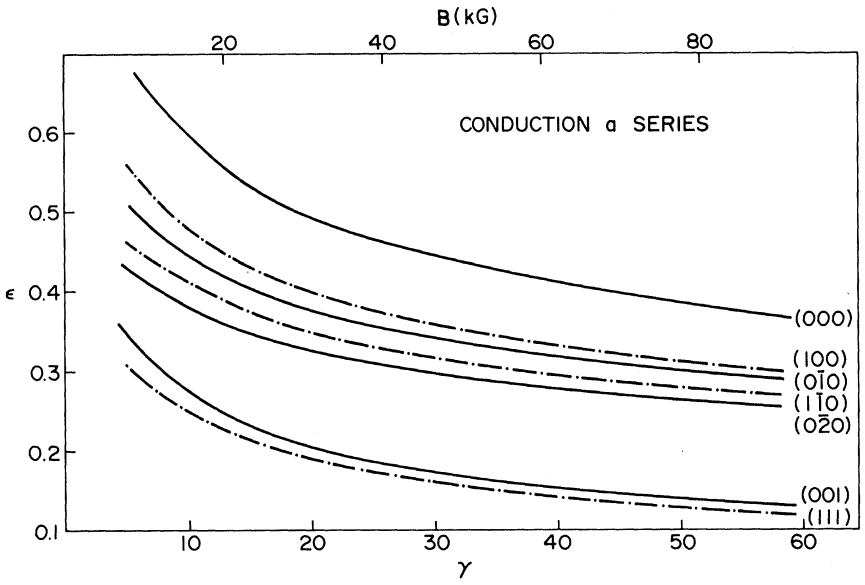

FIG. 2. Variational parameter ϵ as a function of γ for the high field impurity states $(NM\lambda)a$ associated with the conduction a Landau ladder in InSb. Full curves are for $N=0$; dash-dot curves are for $N=1$.

sults are displayed by the curves. The central-cell corrections which were omitted in all the calculations should lower the ground-state energy considerably. It, in turn, should move all the theoretical curves up in Fig. 4. The nonparabolicity effects, on the other hand, result in higher ionization energies for the higher lying states than would be expected from calculations for a simple parabolic band. This effect is most marked for the $(110)a$ state, as compared to the $(001)a$ or the $(0\bar{1}0)a$ state, and is enhanced with increasing field. The evidence for this may be realized from the rapid deviation of the top dashed curve (Wallis-Bowlden parabolic calculation) away from the observed transition energies. The present nonparabolic calculation gives a transition energy $(000)a \rightarrow (110)a$ quite close to the observed value; the small deviation is mainly due to the central-cell effect on the $(000)a$ state. Since the nonparabolic effect for $N=0$ impurity states is not significant (based on the deviation of the theoretical values of the transition energy $(000)a \rightarrow (0\bar{1}0)a$ from the observed value), one can determine the size of central-cell correction needed in each theoretical calculation. We have carried out such a comparison and obtain an H dependence of the ground-state energy correction similar to Larsen's result.

The dashed arrow in Fig. 3 indicates the observed combined resonance transition between the localized electronic states. In Fig. 5, we display by dots the experimental magnetic field dependence of this transition. The splitting of the resonance absorption peak in the magnetic field range $H=30$–40 kOe is due to the strong electron-phonon coupling occurring in that field, region. For comparison, the theoretical result is given by the curve in the same figure. Just as the deviation of the theoretical curve $(000)a \rightarrow (0\bar{1}0)a$ from experiment in Fig. 4 gives the central-cell correction needed for the ground state $(000)a$, so the deviation of $(000)a \rightarrow (110)a$ curve from the dots in Fig. 4 will add information about the amount of nonparabolicity correction left out in this calculation. This follows since we have ignored the odd part, as well as a small anisotropic part of the effective-mass Hamiltonian. Furthermore, the deviation of $(000)a \rightarrow (110)b$ curve from the dots in Fig. 5 will yield information of the amount of spin-orbit interaction left out. As we see, the latter error is rather small.

We want to point out that when we use the type of trial function of Eq. (7), we have assumed that the transverse motion of the electron in a magnetic field is not affected by the impurity potential. Therefore, we have slightly underestimated the binding energy at low fields.

In general, Eq. (9) has not only a set of discrete solutions for which $E(N,M,\lambda)<E(N,M)$, $\lambda=0,1,2,$ ---, but also a continuum solution for which $E(N,M,\nu)>E(N,M)$. Thus the discrete states for $N>0$ will always be degenerate with the continuum state of smaller N value. This means that $(0,M,\lambda)$, $M\leq 0$ are discrete states but, in general, the other states are metastable with rather short lifetimes. However, not all the discrete states for $N>0$ are mixed with the continuum states by the Coulomb term in Eq. (9). The states (N,N,λ) with $N>0$ are degenerate with continuum states (N',M',ν) with $M'<N$, $N'<N$, but the Coulomb matrix elements between them vanish. Thus, these (N,N,λ) states are also discrete and stable.

From the coexisting features of the Rydberg

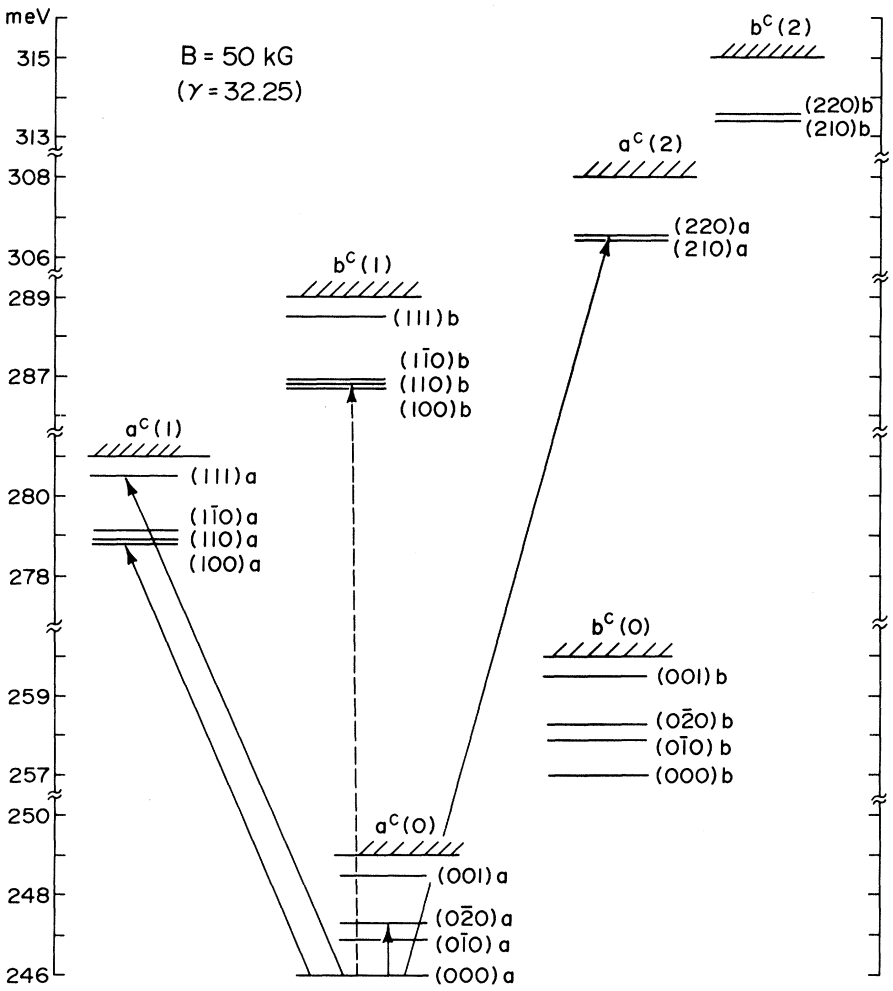

FIG. 3. Energy-level diagram for donor states in InSb at $B = 50$ kG. Arrows show some allowed Raman transitions; dashed arrow indicates the observed combined resonance transition.

series and the Landau levels, the bound electron states at high fields should pass continuously into the Rydberg series in the low-field limit. Previous suggestions concerning the connection between these two series are based on (i) the nodal-surface-conservation argument,[19] and (ii) the noncrossing rule.[20] The former argument gave the following relations for a state $(NM\lambda)$ at high field connecting to a state (nml) of Rydberg series at low field.

$$M = m \tag{16a}$$

$$N - \tfrac{1}{2}(M + |M|) = n - l - 1 \tag{16b}$$

$$\lambda = l - |m| \tag{16c}$$

The first relation (16a) insures angular-momentum conservation, since the Z component of angular momentum is a good quantum number for all field strengths. The second relation (16b) expresses the fact that the number of nodal cylinders of the wave function of $(NM\lambda)$ at $H \to \infty$ is equal to the number of nodal spheres of (nml) at $H \to 0$. The last relation (16c) insures that the number of nodal planes perpendicular to the Z axis for the state (nml) at $H \to 0$ is equal to the number of nodal cones with the Z axis for the state $(NM\lambda)$.

On the other hand, the noncrossing rule simply requires that levels having the same parity and angular momentum cannot be degenerate at any field strength.

The above two suggestions yield quite different level connections. Several level connections based on the first suggestion violate the noncrossing rule. In view of the existing discrepancy, we wish to reexamine carefully these suggestions based on our present calculated level orderings.

Because we have ignored a small inversion-asymmetric odd part in Eq. (1), the effective Hamiltonian in Eq. (9) is invariant under the inversion and rotation operations about the Z axis for all field strengths. The parity and the angular momentum M should then be good quantum numbers, and the noncrossing rule is exact. Accordingly, we make the following connections between the Rydberg series and the truly discrete Landau series.

$1s \rightarrow (000)$, $2s \rightarrow (002)$, $3s \rightarrow (004)$,
$2p_{-1} \rightarrow (0\bar{1}0)$, $2p_0 \rightarrow (001)$, $2p_{+1} \rightarrow (110)$,
$3p_{-1} \rightarrow (0\bar{1}2)$, $3p_0 \rightarrow (003)$, $3p_{+1} \rightarrow (112)$,
$3d_{-2} \rightarrow (0\bar{2}0)$, $3d_{-1} \rightarrow (0\bar{1}1)$, $3d_0 \rightarrow (006)$,
$3d_1 \rightarrow (111)$, $3d_2 \rightarrow (220)$.

It is most interesting to note that, in recent magneto-optic studies of donor excitation spectra in CdTe,[21] the donor levels $3p(m = 0, -1)$ also cross the $2p(m = 1)$ at lower field. The correspondence between low-field and high-field $2p$ and $3p$ levels agrees exactly with the one given above.

The above connections obey the relations in Eqs. (16), except for the cases in which either $n - l - 1 > 0$ or $l - |m| > 1$. The reasons for this may be seen from the following discussion:

(i) As we mentioned, only $(0M\lambda)$ $M \leq 0$ and $(NN\lambda)$ $N \geq 0$ states are truly discrete states. The wave functions of these truly discrete states can not have a nodal cylindrical surface as $H \rightarrow \infty$ because $N - \frac{1}{2}(M + |M|) = 0$ for the truly discrete states. Consequently, as we know that the Rydberg series should always be connected to truly discrete Landau series of bound electrons, Eq. (16b) can never be true for $n - l - 1 > 0$.

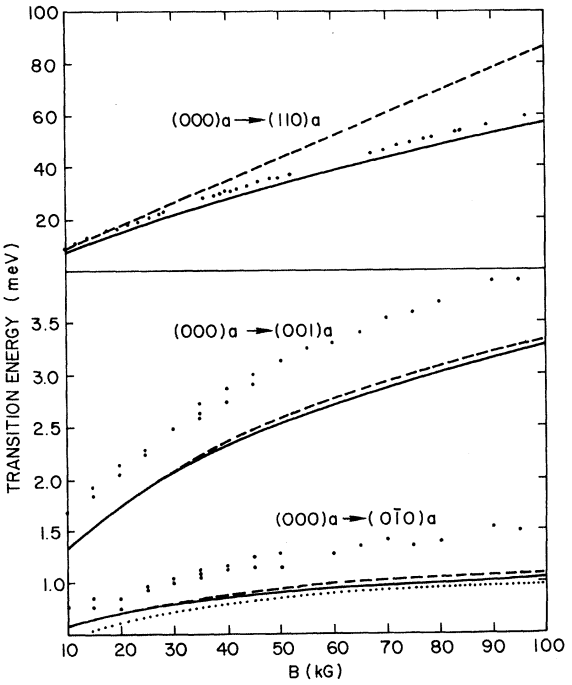

FIG. 4. Field dependence of the three prominent donor-impurity transitions. Observed energies (Ref. 4) are indicated by the black circles. Curves show the following theoretical results: solid curves, present calculation; dashed curves, Wallis and Bowlden (Ref. 8); dotted curve, Larsen (Ref. 9 nonparabolic calculation).

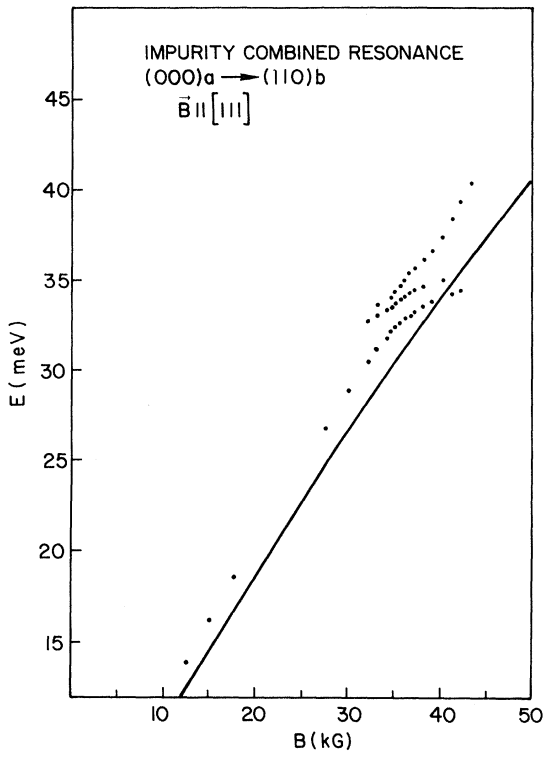

FIG. 5. Observed impurity combined resonance $(000)a \rightarrow (110)b$ (dots) and present theoretical result (curve).

(ii) It is observed that $l - |m| > 1$ occurs only for $l \geq 2$. In fact, we find that Eq. (16c) does not only apply for the cases in which $n - l - 1 = 0$ and $l - |m| > 1$, but also for the case in which $n - l - 1 > 0$.

(iii) In addition, we find that instead of Eq. (16b) and (16c), there exist new relations for the change of number of nodal surfaces of the wave function as (nml) varies into $(NM\lambda)$, namely, the number of nodal spheres which is $n - l - 1$ will change into the number of nodal cylinders, $N - \frac{1}{2}(M + |M|) = 0$; the number of nodal cones which is $l - |m|$ will change into the number of nodal planes $\lambda = l - |m| + 2(n - l - 1)$. The above relation holds for $l - |m| \leq 1$. It seems that whenever some nodal spheres disappear, additional nodal planes emerge perpendicular to the Z axis. The nodal-surface-conservation argument leading to Eq. (16b) and Eq. (16c) is therefore not valid.

IV. HIGH FIELD ACCEPTOR STATES

Unlike free holes in InSb which occupy initial states with multiplicity, bound holes posses unique states. Therefore, it makes the experiments, which involve an acceptor ground state as initial state simpler to study. Because of the degeneracy of the valence-band structure, the acceptor states

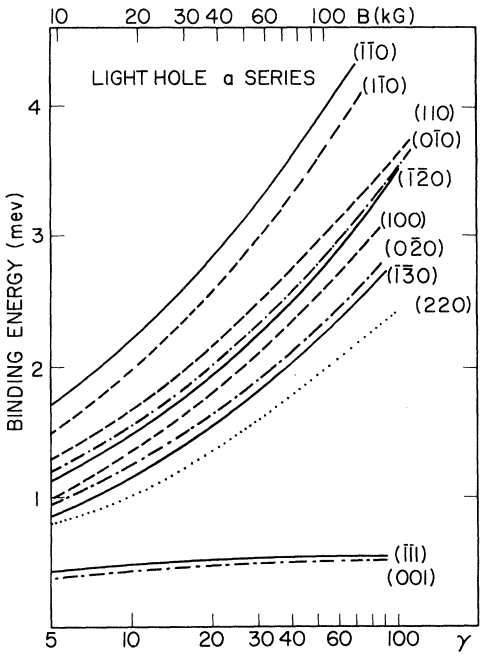

FIG. 6. Binding energy as a function of γ for the high field impurity states $(NM\lambda)a$ associated with the light-hole a Landau ladder in InSb. Full curves are for $N=-1$; dash-dot curves for $N=0$; dashed curves for $N=1$, and dotted curve for $N=2$.

in a magnetic field exist in association with both the low-lying heavy-hole and the widely spaced light-hole Landau ladders. In a magnetic field below a few hundred kG, the cyclotron energy is much greater than the effective Rydberg energy for the light-mass bound hole ($\gamma \gg 1$). The opposite is true for the heavy-mass bound hole ($\gamma \ll 1$). Here, we need only consider the case of light-mass bound holes. The heavy-mass bound hole up to a few hundred kG should follow the result given in the low-field limit.[18]

Again, we have adapted the existing solutions for the Landau ladders associated with free light holes in the magnetic-field range 10 to 100 kOe.[16] Using these solutions, we evaluated Eqs. (12) and (14) for acceptor states associated with both Landau a and Landau b ladders. The results for the magnetic field dependence of acceptor binding energies and variational parameters for the a series are displayed in Figs. 6 and 7. Those for the corresponding states of the b series have a very similar behavior.

The binding energies for the $\lambda=1$ states change very slowly with magnetic field, whereas the $\lambda=0$ states approach infinity as the magnetic field increases. The pairs of states (000) and $(\bar{1}\bar{2}0)$, (001) and (111), $(1\bar{1}0)$ and (010), and (220) and $(0\bar{2}0)$ have binding energies very close to each other, and therefore, only one in each pair is shown in Fig. 6. The binding energies and variational parameters for the acceptor states at $H=50$ kOe are listed in Table III. The energy-level diagram is given in Fig. 8 where the zero of energy is the position of the valence-band edge at zero field. In this diagram, the ordering for the states in the a series and b series remain the same, and the binding energies for the corresponding levels in these two series are quite close. The magneto-oscillatory excitation spectra of acceptor impurities in

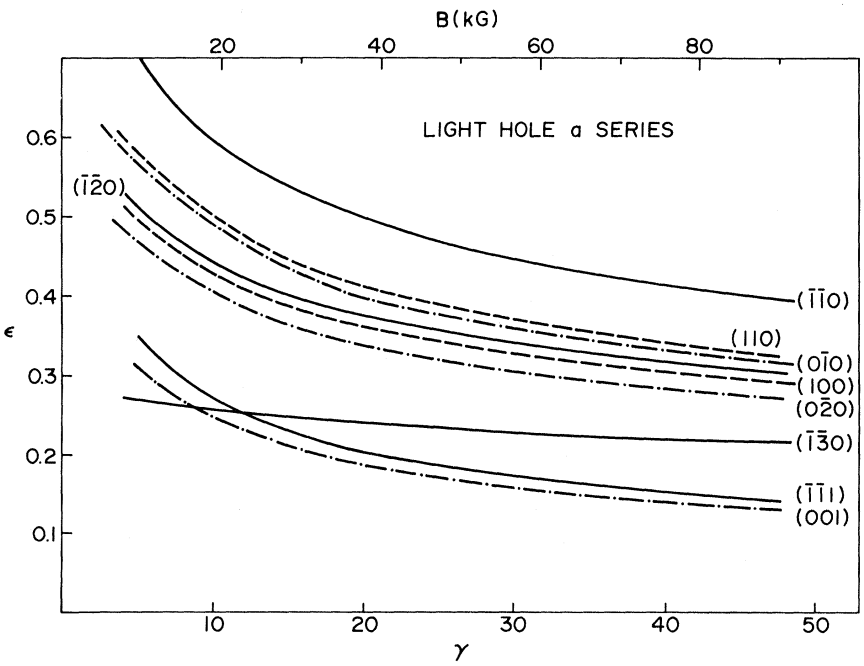

FIG. 7. Variational parameter ϵ as a function of γ for the high field impurity states $(NM\lambda)a$ associated with the light-hole a Landau ladder in InSb. Full curves are for $N=-1$; dash-dot curves for $N=0$, and dashed curves for $N=1$.

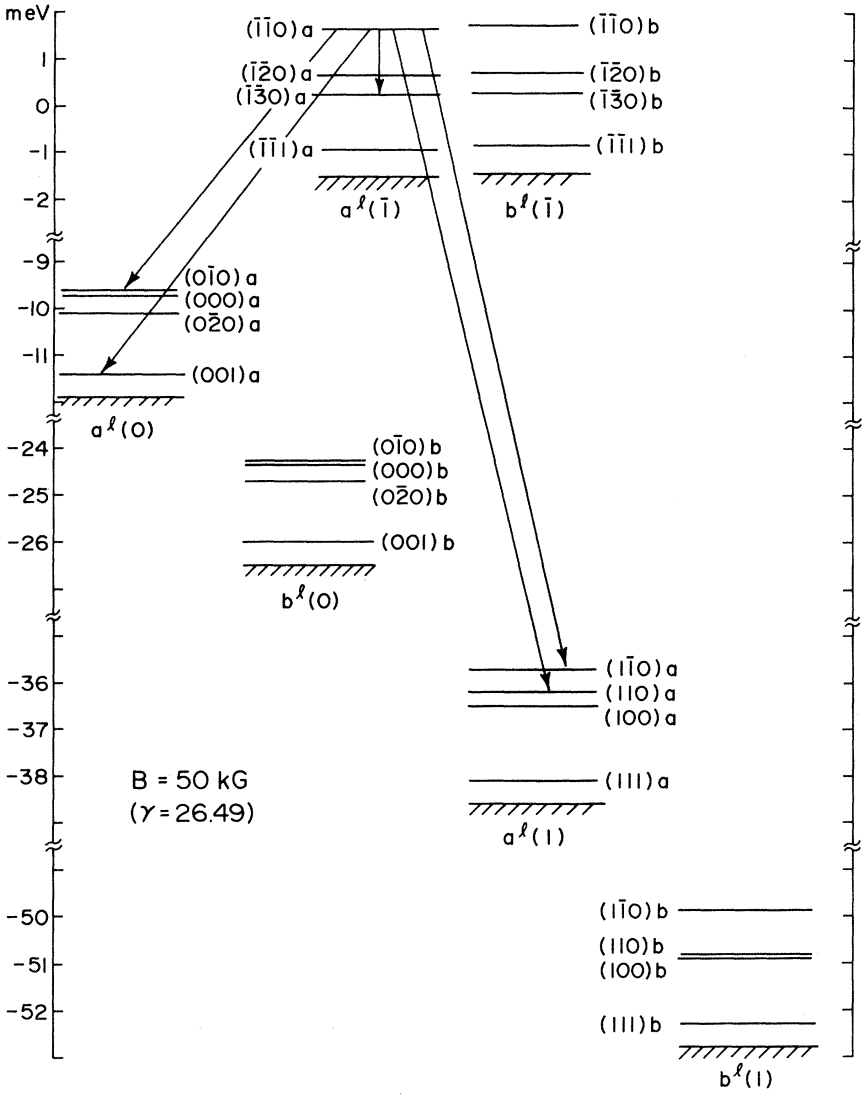

FIG. 8. Energy-level diagram for light-hole acceptor states in InSb at $B = 50$ kG. Arrows show some allowed Raman transitions between bound-hole states.

Ge (Ref. 3) show many transmission minima representing transitions from the s-like (heavy-mass) acceptor ground state into p-like impurity excited states associated with the light-hole Landau ladder. The binding energies of the p-like excited states are observed to increase monotonically with increasing H and to decrease with increasing N for $N < 7$. Unfortunately, observation of this kind of result was not achieved for the InSb spectra because of poorer resolution relative to that of the Ge spectra. Thus a quantitative comparison with experiment cannot be made for the time being. However, the binding energies of the p-like excited states $(\bar{1}20)$, (000), (100), (220) do show an increase with increasing field and a decrease with increasing N (except for the $N = -1$ state).

It is extremely difficult to connect the light-hole Landau series $(NM\lambda)^l$ with the bound-hole states as $H \to 0$. Because the valence-band edge is degenerate at zero field, there is strong mixing of the light-hole and heavy-hole character in each component of the Γ_8, Γ_6, Γ_7 bound-hole states.[18] In addition, because the valence-band edge is p like in character, the bound-hole states Γ_8 etc. have mixed atomic characters, s with d, or p with f. Similarly, at high field, by comparing the coefficients A_3 with A_5 in Table I, we can see that the states in the Landau series $(NM\lambda)^l$ also contain a large portion of heavy-hole wave function in the expansion of Eq. (5) for the $N \geq 1$ light-hole subbands. It is then a formidable task to connect the two sets of levels at $H \to 0$ and $H \to \infty$. However, for the same reason as we gave in Sec. III, we know that the only truly discrete states for the $(NM\lambda)^l$ series are $(\bar{1}M\lambda)$ and $(NN\lambda)$, in which $N > -1$ and only these states are connected to the

TABLE III. Binding energies and variational parameters for the impurity levels at $B=50$ kG (energy is in meV; the first three columns are for donors, the rest are for acceptors).

$(NM\lambda)^c$	E_B	ϵ	$(NM\lambda)^l$	E_B	ϵ
$(0\,0\,0)a$	3.0071	0.4353	$(\bar{1}\,\bar{1}\,0)a$	3.1356	0.4622
$(0\,\bar{1}\,0)a$	2.1041	0.3357	$(\bar{1}\,\bar{2}\,0)a$	2.1558	0.3514
$(0\,\bar{2}\,\bar{0})a$	1.7368	0.2918	$(\bar{1}\,\bar{3}\,0)a$	1.7219	0.2333
$(0\,0\,1)a$	0.4763	0.1672	$(\bar{1}\,\bar{1}\,1)a$	0.5197	0.1823
$(0\,0\,0)b$	2.9606	0.4306	$(\bar{1}\,\bar{1}\,0)b$	3.1356	0.4622
$(0\,\bar{1}\,0)b$	2.1084	0.3366	$(\bar{1}\,\bar{2}\,0)b$	2.1558	0.3514
$(0\,\bar{2}\,0)b$	1.7396	0.2924	$(\bar{1}\,\bar{3}\,0)b$	1.7219	0.2333
$(0\,0\,1)b$	0.4754	0.1668	$(\bar{1}\,\bar{1}\,1)b$	0.5197	0.1823
$(1\,0\,0)a$	2.1400	0.3500	$(0\,\bar{1}\,0)a$	2.2235	0.3719
$(1\,1\,0)a$	2.1373	0.3399	$(0\,0\,0)a$	2.1799	0.3546
$(1\,\bar{1}\,0)a$	1.8830	0.3102	$(0\,\bar{2}\,0)a$	1.8132	0.3169
$(1\,1\,1)a$	0.4502	0.1572	$(0\,0\,1)a$	0.4874	0.1701
$(1\,0\,0)b$	2.1139	0.3472	$(0\,0\,0)b$	2.2296	0.3606
$(1\,1\,0)b$	2.0730	0.3322	$(0\,\bar{1}\,0)b$	2.2249	0.3711
$(1\,\bar{1}\,0)b$	2.0519	0.3226	$(0\,\bar{2}\,0)b$	1.8153	0.3165
$(1\,1\,1)b$	0.4478	0.1563	$(0\,0\,1)b$	0.4905	0.1709
$(2\,1\,0)a$	1.7993	0.3063	$(1\,\bar{1}\,0)a$	2.8580	0.3837
$(2\,2\,0)a$	1.7605	0.2947	$(1\,1\,0)a$	2.3963	0.3837
			$(1\,0\,0)a$	2.0169	0.3396
			$(1\,1\,1)a$	0.4519	0.1715
$(2\,1\,0)b$	1.7514	0.3001	$(1\,\bar{1}\,0)b$	3.7273	0.4366
$(2\,2\,0)b$	1.7153	0.2893	$(1\,1\,0)b$	1.9546	0.3289
			$(1\,0\,0)b$	1.9075	0.3290
			$(1\,1\,1)b$	0.4729	0.1645
			$(2\,1\,0)a$	1.7568	0.3355
			$(2\,2\,0)a$	1.7119	0.3203
			$(2\,1\,0)b$	1.5457	0.3034
			$(2\,2\,0)b$	1.5147	0.2927

low-field acceptor states.

V. OPTICAL AND RAMAN TRANSITIONS BETWEEN IMPURITY STATES IN A MAGNETIC FIELD

The optical absorption coefficient associated with transitions from an initial state i to a final state j, in the absence of any broadening can be written

$$\alpha(\omega)=8\pi^3(n/Khc)N_i\sum_j (E_j-E_i)\,|P_\mu|^2 \times\delta(E_i-E_j+\hbar\omega)\,, \tag{17}$$

where n, K are the refractive index and dielectric constant of the material, N_i is the concentration of impurity atoms in the initial state, ω is the frequency of the radiation, E_i, E_j are, respectively, the energies of initial and final state. P_μ has the following expression

$$P_\mu=e\int F_i^*(\vec{r})\,\mu\,F_j(\vec{r})\,d\vec{r}\,, \tag{18}$$

where F_i, F_j are the effective-mass functions of the initial and final state, μ is the coordinate vector in the direction of the electric vector of the plane polarized radiation or represents $\frac{1}{2}(X+iY)$ and $\frac{1}{2}(X-iY)$ for left and right circularly polarized radiation (if the magnetic field is in the Z direction).

By evaluating the quantity P_μ, we will be able to determine the selection rule for an optical absorption transition between two discrete states. The selection rule for the transition between acceptor states is the same as that between donor states,

For plane-polarized radiation with $\vec{\epsilon}\parallel\vec{H}$,

$$\Delta N=0,\quad \Delta M=0,\quad \Delta\lambda \text{ odd}.$$

For circularly polarized radiation with $\vec{S}\parallel\vec{H}$,

$$\Delta N=0 \text{ or } \pm1,\quad \Delta\lambda \text{ even},\quad \Delta M=\pm1$$

(ΔM positive for left circularly polarized radiation, ΔM negative for right circularly polarized radiation).

The above selection rule holds for $\gamma\gg1$. For arbitrary large magnetic field, the effective-mass wave function will not be in the form of Eq. (7) but rather a linear combination of functions $F(N, M, \lambda)$ with different N values. However M and λ remain good quantum numbers, and therefore, the optical transition will be possible between the states with proper M and λ values, regardless of the N value.

While optical transitions link states with opposite parities, the Raman transition, being a second-order effect, links states with the same parity.

Throughout this paper, we have ignored a small inversion-asymmetric term in the effective-mass Hamiltonian for the zinc-blende crystals. Thus, the selection rules so derived give strong allowed transitions. Inversion-asymmetry-induced transitions should give a weak structure in the observed spectra. The cross section for the strong Raman scattering in the dipole approximation is proportional to the following quantity:

$$W=\frac{\omega_F}{\omega_I}\left|A_{fi}\right|^2 =\frac{\omega_F}{\omega_I}\left|\frac{1}{m}\sum_\gamma \frac{(\vec{\epsilon}_F^{\,*}\cdot\vec{\pi})_{f\gamma}(\vec{\epsilon}_I\cdot\vec{\pi})_{\gamma i}}{E_i+\hbar\omega_I-E_\gamma} +\frac{(\vec{\epsilon}_I\cdot\vec{\pi})_{f\gamma}(\vec{\epsilon}_F^{\,*}\cdot\vec{\pi})_{\gamma i}}{E_i-\hbar\omega_F-E_\gamma}\right|^2 \tag{19}$$

Here $\vec{\pi}=\vec{p}+(e/c)\vec{A}$; i, γ, f label, respectively, the initial, intermediate, and final states; $\vec{\epsilon}_I$, $\vec{\epsilon}_F$, ω_I, ω_F are the polarizations and frequencies of the incident and emitted radiation; m is the free-electron mass.

By computing Eq. (19), we have found the selection rule for Raman transitions, which is shown in Table IV. In Figs. 3 and 8, the solid arrows show some allowed Raman transitions between the bound-electron states and the bound-hole states, respectively. The $(100)a$ state in Fig. 3 and $(1\bar{1}0)a$,

TABLE IV. Selection rules for Raman transitions between the impurity levels in InSb in a magnetic field.

$\Delta\lambda$	ΔN	ΔM	ϵ_I	ϵ_F
even	0	0	$\vec{\epsilon}_I \parallel \vec{H}$	$\vec{\epsilon}_F \parallel \vec{H}$
	$0 \pm 1, \pm 2$	$0, \pm 2$	$\vec{\epsilon}_I \perp \vec{H}$	$\vec{\epsilon}_F \perp \vec{H}$
odd	$0, \pm 1$	± 1	$\vec{\epsilon}_I \perp \vec{H}$	$\vec{\epsilon}_F \parallel \vec{H}$
			$\vec{\epsilon}_I \parallel \vec{H}$	$\vec{\epsilon}_F \perp \vec{H}$

$(0\bar{1}0)a$ states in Fig. 8 are metastable states; the transitions to these states are broadened by interaction with the continuum states having smaller N values.

Recently Hasegawa and Howard found that when the Coulomb perturbation of the continuum states near the Landau-level edges is taken into account properly, the magnitude of optical absorption per unit energy at a Landau edge will tend to zero at $H \to \infty$. In this limit, the optical transition to bound states beneath the Landau edges become intense. Magneto-optical absorption experiments also support this interpretation. Therefore, one would expect that at extremely high fields, the intense prominent peaks in the optical spectrum should correspond to transitions to bound states well separated from Landau edges.

The experimental observation of impurity-shifted Raman lines in high magnetic field is most favorable for donors in InSb. However, ordinarily, the donor concentrations are as low as $10^{14}/\text{cm}^3$. At such low concentration, the intensity may not be sufficiently high. Thus, high magnetic fields are most desirable in detecting the difference in frequency for the Raman lines, respectively associated with bound-carrier and free-carrier transitions.

In conclusion, we have made a survey of the high-field impurity states in InSb by considering nonparabolic band effects and band-band interaction. The warping, as well as the complexity of the valence band, are included in the determination of the donor and acceptor states in high field. By quantitatively comparing our calculated results with the experimentally determined values, we have found the magnitude of the central-cell correction and a small amount of nonparabolic effects left out in this effective-mass-approximation calculation. For typical circumstances, in InSb, the energy gap E_G is much greater than the Landau-level spacing, and the carrier concentration is low enough so that the effective Bohr radius is small compared with the average distance between the impurity centers. Under these conditions, the isolated-hydrogenic-impurity model treated in the effective-mass approximation yields results which can explain the available experimental data very well.

[1] L. J. Neuringer, Phys. Rev. Lett. 18, 773 (1967).
[2] Y. Yafet, R. W. Keyes, and E. N. Adams, J. Phys. Chem. Solids 1, 137 (1956).
[3] R. Kaplan, Phys. Rev. Lett. 20, 329 (1968).
[4] R. Kaplan, Phys. Rev. 181, 1154 (1969).
[5] R. Kaplan and R. F. Wallis, Phys. Rev. Lett. 20, 1499 (1968).
[6] B. D. McCombe and R. Kaplan, Phys. Rev. Lett. 21. 756 (1968).
[7] R. Kaplan, K. L. Ngai, and B. W. Henvis, Phys. Rev. Lett. 28, 1044 (1972).
[8] R. F. Wallis and H. J. Bowlden, J. Phys. Chem. Solids 7, 78 (1958).
[9] D. M. Larsen, J. Phys. Chem. Solids 29, 271 (1968).
[10] M. Von Ortenberg, J. Phys. Chem. Solids 34, 397 (1973).
[11] H. Hasegawa, *Physics of Solids in Intense Magnetic Fields*, edited by E. D. Haidenmenakis (Plenum, New York, 1969).
[12] C. R. Pidgeon and R. N. Brown, Phys. Rev. 146, 575 (1966).
[13] C. R. Pidgeon and S. H. Groves, Phys. Rev. 186, 824 (1969).
[14] J. M. Luttinger and W. Kohn, Phys. Rev. 97, 869 (1955).
[15] The odd part is the interaction term linear in k which is zero for materials with inversion symmetry. The small anisotropic part, which we ignored in our calculation, is the part which gives anisotropic effective mass in the plane perpendicular to the external magnetic field.
[16] We thank Dr. S. H. Groves for sending us the refined unpublished results which we use in our calculation.
[17] A. Baldereschi and F. Bassani, *Proceedings of the Tenth International Conference on the Physics of Semiconductors, Cambridge, Mass.* (U. S. AEC, Washington, D. C., 1970).
[18] P. J. Lin-Chung and B. W. Henvis (unpublished).
[19] R. J. Elliott and R. Loudon, J. Phys. Chem. Solids 15, 196 (1960).
[20] W. S. Boyle and R. E. Howard, J. Phys. Chem. Solids 19, 181 (1961).
[21] R. J. Wagner and B. D. McCombe, Phys. Status. Solidi B 64, 205 (1974).